Nanomanufacturing with DNA Origami: Factors Affecting the Kinetics and Yield of Quantum Dot Binding

*Seung Hyeon Ko, Gregg M. Gallatin, and J. Alexander Liddle**

Molecularly directed self-assembly has the potential to become a nanomanufacturing technology if the critical factors governing the kinetics and yield of defect-free self-assembled structures can be understood and controlled. The kinetics of streptavidin-functionalized quantum dots binding to biontinylated DNA origami are quantitatively evaluated and to what extent the reaction rate and binding efficiency are controlled by the valency of the binding location, the biotin linker length, and the organization, and spacing of the binding locations on the DNA is shown. Yield improvement is systematically determined as a function of the valency of the binding locations and as a function of the quantum dot spacing. In addition, the kinetic studies show that the binding rate increases with increasing linker length, but that the yield saturates at the same level for long incubation times. The forward and backward reaction rate coefficients are determined using a nonlinear least squares fit to the measured binding kinetics, providing considerable physical insight into the factors governing this type of self-assembly process. It is found that the value of the dissociation constant, K_d, for the DNA–nanoparticle complex considered here is up to seven orders of magnitude larger than that of the native biotin–streptavidin complex. This difference is attributed to the combined effect that the much larger size of the DNA origami and the quantum dot have on the translational and rotational diffusion constants.

1. Introduction

DNA generates molecularly precise nanostructures[1] that can serve as templates for the hierarchical assembly of additional nanoscale components[2,3] into more complex, functional devices. DNA origami[4] is a particularly attractive vehicle for this purpose, being readily configurable into different geometries and easily functionialized to provide a diverse set of binding sites. Origami can themselves be assembled into larger structures[5–7] and precisely located on templating surfaces[8] to create more extended devices or arrays of devices. Finally, they have the potential to be synthesized in large quantities using simple, solution-based methods at room temperature. All of these factors suggest that DNA origami may be a viable nanomanufacturing platform. As a result, there has been intense activity in this area and a number of methods have been developed, using DNA origami–nanoparticle conjugates, to construct a variety of nanoarchitectures.[9–16] Despite the variety of structures being fabricated, there appear to be common issues related with the poor yields. In this work we therefore seek to explore and understand the factors that control the kinetics and the yield. One common method is to use DNA hybridization to attach nanoparticles (NPs) to origami templates, which, although attractive because it provides site specificity, has resulted in poor yields of the desired NP-DNA conjugates.[12] Yields can be improved by incorporating multiple interaction sites at a given attachment location, but the absolute yields remain low.[9,13,15,16] In order to achieve reproducibly high yields of precisely constructed nanoarchitectures it is important to understand quantitatively the interplay of the diverse factors that affect the binding of nanoparticles to DNA origami. This can be effected by developing metrics to determine the strength and number of binding sites, the optimal linker length, and the minimum binding location separation at a given attachment location necessary to meet a specific yield target.

Here, the necessary metrics are developed by applying statistical methods to kinetic data for binding of streptavidin-functionalized quantum dots (Qdots) to biotinylated DNA origami. Binding probabilities as a function of time are extracted from atomic force microscopy (AFM) images and are then used to determine the extent to which linker length, binding site valency, and binding site separation affect the formation of complex nanostructures.

Of particular note, we find that the dissociation constant of the biotinylated DNA origami:streptavidin-Qdot complex is orders of magnitude larger than that reported for the free biotin-streptavidin complex, a result we attribute to differences in the translational and rotational diffusion constants between the two systems.

Dr. S. H. Ko
Center for Nanoscale Science and Technology
National Institute of Standards and Technology
Gaithersburg, MD 20899
Institute for Research in Electronics and Applied Physics
University of Maryland, College Park, MD 20742
Dr. G. M. Gallatin, Dr. J. A. Liddle
Center for Nanoscale Science and Technology
National Institute of Standards and Technology
Gaithersburg, MD 20899
E-mail: liddle@nist.gov

DOI: 10.1002/adfm.201102077

2. Results and Discussion

2.1. Formation of Qdot Nanopatterns

2.1.1. Choice of Binding Partners

We chose the binding of streptavidin-functionalized Qdots to biotinylated sites on DNA as a model system because the streptavidin–biotin interaction is strong, generally applicable and well-studied.[17–20] Streptavidin is a tetrameric protein that binds biotin in solution with extraordinarily high affinity (dissociation constant $K_d = 10^{-15}$ mol L^{-1}),[20] as compared to, for example, duplex DNA, which has a K_d of 6.7×10^{-10} mol L^{-1} for a 10-mer with 1 mol L^{-1} NaCl at ≈30 °C.[21] A degree of freedom is provided by varying the number of biotins at each binding location on the DNA. Each Qdot has an approximate diameter of 20 nm and is functionalized with an average of 5 to 10 streptavidins.[22,23] Such a strong linker system should, in principle, produce intrinsically high yields that allow for the unambiguous separation of affinity from other yield-influencing factors. It also provides the opportunity for investigating the impact of the DNA and Qdots on the stability of the streptavidin–biotin complex because the binding efficiency is decreased when either partner is attached to a larger object.[24–30]

2.1.2. Design of DNA Origami Template

To investigate the influence of binding location separation, and hence steric hindrance, on the yield of the Qdot–DNA complex we used a rectangular shaped origami template,[4] 100 nm × 70 nm, separately synthesizing templates with three different patterns of biotinylated binding locations (**Figure 1**), with spacings of 50 nm (Design I), 35 nm (Design II), and 22 nm (Design III). To test the effect of binding site valency on yield, monovalent and trivalent binding sites were used. In this case, we synthesized two versions of the origami templates described above, with either one or three biotinylated sites at each binding location. These sites were introduced by replacing selected staple strands by 5′-biotin conjugated strands. Trivalent binding locations consist of adjacent biotins arranged on the vertices of an equilateral triangle approximately 5 nm on a side. This spacing is small enough to allow multivalent interactions between a single Qdot and a binding location, but large enough to preclude multivalent interactions with a single streptavidin, since the spacing between the streptavidin binding pockets is only 2 nm.[17] The sequences of the biotin-conjugated strands are the same as the corresponding unmodified staple strands except that they have an extra spacer of thymines close to the 5′-biotin conjugation. The spacer length was varied from four thymines (4T) to ten thymines (10T) to explore the influence of spacer length on the kinetics and yield.

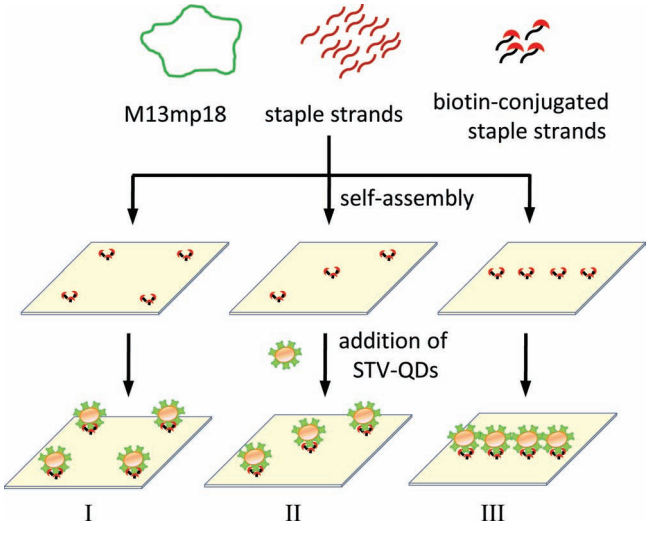

Figure 1. Schematic representation of the fabrication process of Qdot nanopatterns on DNA origami templates. Groups of three biotin-conjugated staple strands were located at predetermined binding sites to capture streptavidin (STV)-conjugated Qdots (QDs). The distance between adjacent binding sites was 50 nm (I), 35 nm (II), and 22 nm (III).

We used origami with a staggered merge pattern, so that all modifications made to the middle of a staple strand lie on the same face of the lattice.[4] We used a common protocol to load the origami onto mica substrates and verified that it led to more than 90% of the origami having the conjugated biotins facing up (Supporting Information, Figure S1), consistent with previous observations.[31–33] We tested the accessibility of the biotinylated sites on the DNA origami by adding streptavidin to single biotin-conjugated DNA origami templates. The specific binding of streptavidin on DNA origami was clearly observed (**Figure 2**), with high yields and with binding positions consistent with the designed binding locations for all three binding location separations. Consistent with a previous report,[14] the height change that occurred upon streptavidin binding was measured to be 0.67 nm ± 0.16 nm by cross-section profile analysis of our AFM images (Supporting Information, Figure S2).

Qdot nanopatterns on DNA origami were constructed by adding an excess quantity (15:1 (Qdot:binding location) molar ratio) of streptavidin-coated CdSe/ZnS core/shell Qdot[34] directly to origami templates immobilized on a mica surface. Under these conditions, and at room temperature, an incubation time of approximately 15 h (900 min) was sufficient to ensure that equilibrium was reached and was therefore used unless otherwise stated. Designs I and III have four binding locations. Design II has three. The AFM images (**Figure 3**) clearly show that streptavidin-coated Qdots bind specifically to the biotinylated locations on the templates. As a control, we mixed Qdots with non-biotinylated DNA origami templates and observed no interaction.

2.1.3. Binding Efficiency

In order to generate the data for quantitative analysis, we first determined the binding frequency for each design by manually counting the number of Qdots bound to each origami in each AFM image. The frequency with which origami with 0, 1, 2, 3, or 4 occupied sites occur is then used to calculate the probability of occupation, or the binding efficiency, pocc, for a single site by fitting the data to a binomial distribution.

2.2. Trivalent versus Monovalent Interaction

To assess the effect of trivalent (3B) versus monovalent (1B) binding locations on the yield of bound Qdots, we use a

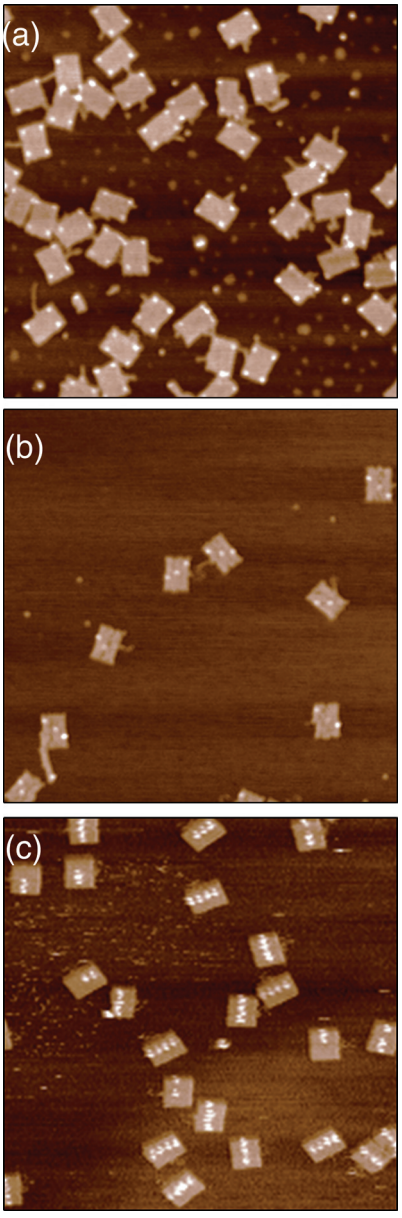

Figure 2. Streptavidin binding on predefined singly biotinylated binding locations on DNA origami template. a) Design I, b) Design II, and c) Design III observed after an incubation time of 180 min.

quantitative comparison of yield distribution data for the three different designs, shown in **Figure 4**, (additional AFM images of larger areas for each case are provided in the Supporting Information, Figure S6, S7, S8). For Design I, the yield of the desired tetramer pattern increased from 22.1% ± 6.5% (mean ± 1σ with σ the root-mean-square variation) for the monovalent case to 90.2% ± 3.3% for the trivalent case. The probability of occupation for a single site or the binding efficiency, p_{occ}, increased from 70.0% ± 1.6% for the monovalent case to 97.6% ± 0.8% for the trivalent case (Supporting Information, Figure S3). For Design II (Figure 4), the desired trimer pattern predominated (54.3% ± 6.1%) for the 3B-DNA origami whereas the 1B-DNA origami produced mainly dimers (47.9% ± 8.7%). Similarly, Design III (Figure 4) generated 19.5% ± 4.9% of the designed tetramer Qdot pattern for the 3B-DNA origami, while more than 90% of the corresponding 1B-DNA origami had only monomer or dimer patterns. The calculated p_{occ} for 3B-origami was 81.8% ± 2.6% for Design II, falling to 71.5% ± 2.0% for Design III, while the corresponding 1B-origami templates displayed significantly lower binding efficiencies of 58.2% ± 5.3% for Design II and 40.0% ± 1.4% for Design III. As expected, increasing the number of binding sites at a binding location leads to higher yields. We attribute this improvement to both the increased binding probability offered by the effectively larger trivalent binding locations, as well as to the possibility of multiple biotin interactions with the same Qdot. However, as we highlight below, increasing binding site valency does not guarantee perfection in the resulting nanostructure.

2.3. Steric Effects

Design I has the largest binding location spacings: 50 nm along the 70 nm side and 65 nm along the 100 nm side of the origami. As discussed above, in the case of trivalent binding locations, a high yield of Qdots bound to each location on a template was observed, generating a rectangular tetramer pattern (Figure 3). The average spacings (mean ± 1σ) between Qdots measured from AFM images were 52.7 nm ± 4.3 nm and 70.1 nm ± 5.9 nm along the 70 nm and 100 nm sides, respectively. These measurements show good agreement with the design parameters and are consistent with the small displacements observed in the images presented by other workers.[9,11,14] For Design II (35 nm designed spacing), we observed trimer patterns of Qdots with an average spacing of 40.8 nm ± 6.0 nm, but the Qdots were not always arrayed linearly along the diagonal of the origami. Based on the statistical analysis presented below we believe this is primarily an artifact induced by capillary forces acting during drying. Design III (22 nm designed spacing) generated predominantly trimer Qdot patterns, with Qdot-to-Qdot separations of 42.1 nm ± 5.0 nm, which is double the spacing expected for this design. We occasionally observed tetramers with center-to-center distances of 31.7 nm ± 7.2 nm. The extent of the displacements from the designed positions becomes larger as the spacing between binding locations is reduced from Design II to III. In addition, we observe significant and frequent distortions of the origami template occurring for the smallest binding location spacing. In contrast to these observations, as mentioned above, a control experiment of streptavidin binding to DNA origami templates with singly biotinylated binding locations showed no significant difference in binding efficiency between the three different designs. In addition, streptavidin was observed to bind with high yield and placement accuracy to all the predesigned binding locations, even at the smallest spacing (22 nm) in Design III. This result is consistent with the previously reported observations allowing for the differences in experimental conditions and design of binding systems.[35]

The influence of sterics on binding was quantified by comparing the distribution of bound Qdots against the fit binomial distribution. It should be noted that in all cases the values of p_{occ} computed by fitting to the binomial distribution were

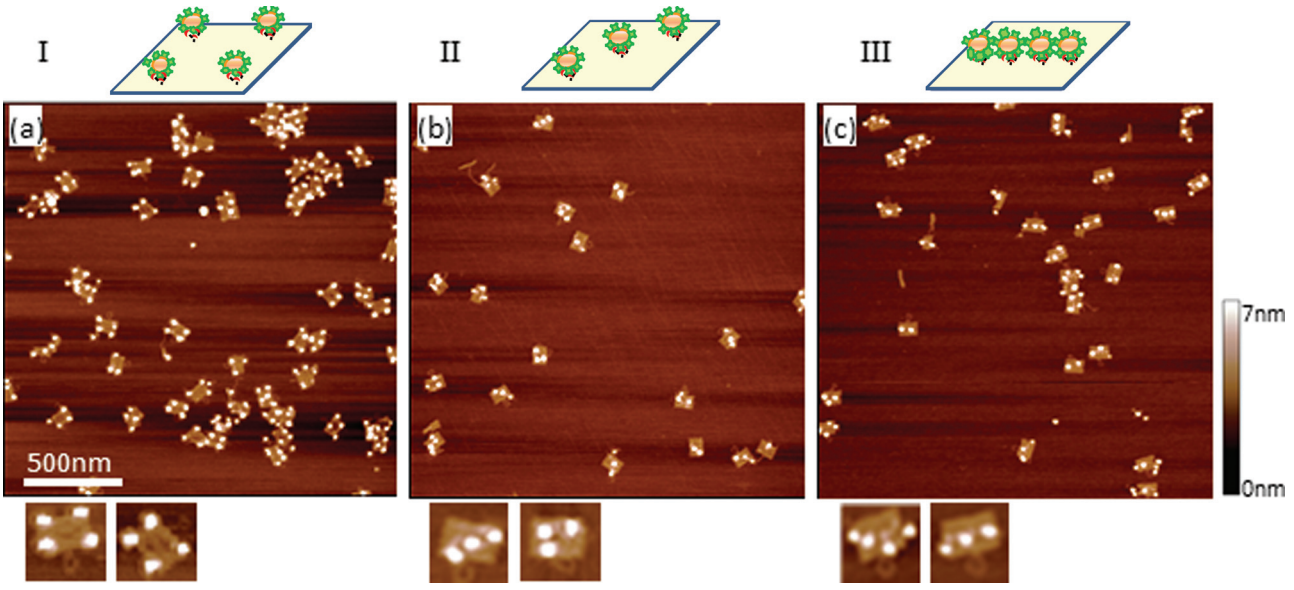

Figure 3. AFM images of Qdot nanopatterns on DNA origami templates containing three biotins per binding location. Three different Qdot nanopatterns (Design I, II, and III) were interrogated. The topographic illustration of each design and its corresponding AFM image are shown. Two magnified images of individual DNA origami are below each larger image.

virtually identical to the overall percentage of occupied sites, as expected. The binomial distributions computed for Design II using the calculated values of p_{occ} fit the measured data to within the error bars, suggesting that the reduced occupation probability relative to Design I is a result only of a reduction in the binding rate relative to the unbinding rate. However, for Design III it is clear that the binomial distributions computed using the calculated values of p_{occ} do not fit the data which is consistent with the large degree of pattern distortion. The trimer and tetramer states in the 1B-DNA origami and the tetramer state in the 3B-DNA origami are under occupied. This has the effect of pushing the distribution to lower occupancy states since the sum of the percentages of bound Qdots is always 100%.

The deviation of the site occupation data from the expected distribution, combined with the observed displacement of the bound Qdots from the designed positions for Design III suggest that electrostatic and/or steric effects between neighboring Qdots become significant as the binding location spacing tends towards the size of the Qdots.[34]

2.4. Binding Kinetics

In order to quantitatively determine the reaction rate constants of the Qdot-origami self-assembly process, we measured the binding yield as a function of incubation time. Yield data were collected for the 3B-DNA, Design I. **Figure 5** shows histograms of the binding location occupancy per template at different incubation times along with the calculated values of p_{occ} for each. The distribution shifts to higher values with increasing incubation time, peaking at two Qdots per origami after 60 min of incubation and rising to an equilibrium value of four dots with 97.6% ± 0.8% yield after 900 min. Again, a fit to the binomial distribution for each sample in the time course showed that, for the trivalent Design I, the binding locations act independently with an equal attachment probability.

Although the binding of native streptavidin and biotin is very efficient and stable,[17,18] we find that the binding reaction rate decreases significantly if the streptavidin and/or biotin are attached to Qdots and DNA origami respectively. Under similar buffer conditions, the binding of free streptavidin and biotin in solution would be almost complete in less than 1 min, a factor of 1000 times faster. Clearly, the reaction rates for the free species cannot be used to determine appropriate reaction times when these same binding partners are attached to bulky species.

The forward and backward rate constants and their 1σ uncertainties are determined using the best fit p_{occ} data and the 1σ uncertainties in p_{occ} derived from the fit for the binding process, which can be represented as

$$[\text{Qdot}] + [\text{DNA}] \underset{k_b}{\overset{k_f}{\leftrightarrows}} [\text{Qdot DNA}] \quad (1)$$

Here k_f and k_b are the forward and backward rate constants, respectively, and [Qdot], [DNA], and [Qdot DNA] represent the concentrations of Qdots, DNA origami, and bound species, respectively. Note that k_f has units of volume (mole × time)$^{-1}$ whereas k_b has units of time^{-1}. In our experiments the initial Qdot concentration is much larger than the initial DNA concentration and so the maximum possible concentration of Qdot-DNA complexes is the same as the initial DNA concentration. Although there is some ambiguity in determining the actual value of the DNA concentration (see Experimental Section) the fits of $C(t)$ to the p_{occ} data were found to be insensitive to variations in this parameter. Thus the fraction of bound sites or binding efficiency as a function of time, $p_{occ}(t)$, is given by

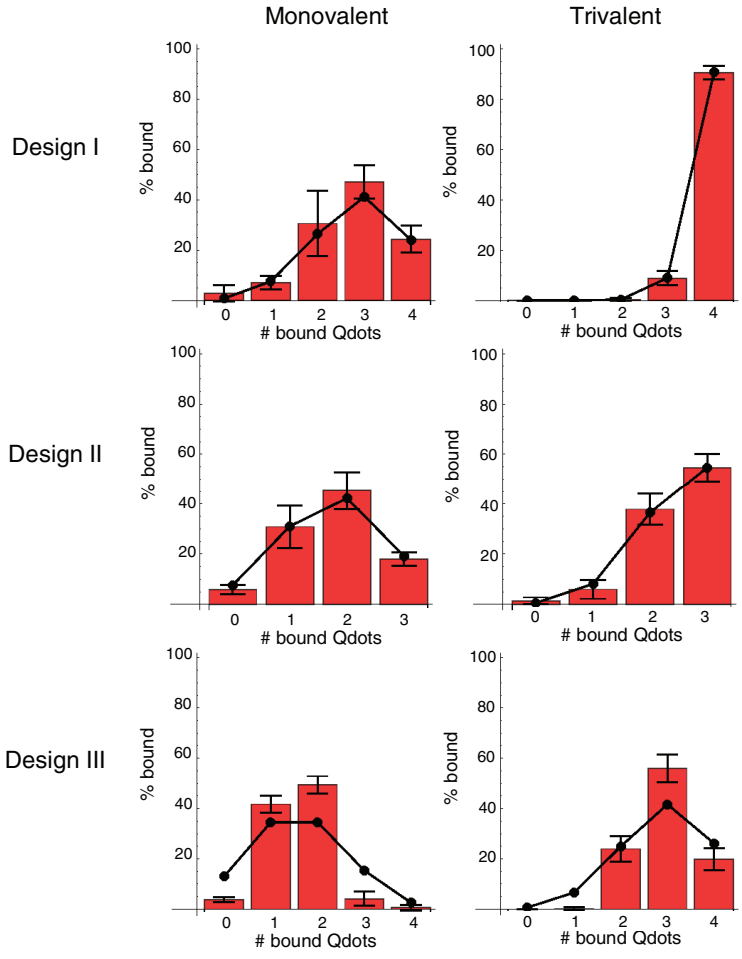

Figure 4. Histogram (bars) for the yield of Qdot-nanopatterns of 1B-origami (Monovalent) and 3B-origami (Trivalent) for Design I, II, and III. Data were collected from AFM images of more than 240 origami pieces for each case. The 1 σ variation in the data is shown as error bars. The dots are the binomial distribution for the value of p_{occ} determined by fitting the data. The lines are meant as a guide to the eye.

$$p_{occ}(t) = \frac{C(t)}{C_{DNA0}} \quad (2)$$

where $C(t)$ is the concentration of bound sites as a function of time t and C_{DNA0} is the initial concentration of DNA. Details of the error analysis are provided in the Supporting Information. As a guide to interpreting the results presented below, k_f depends predominantly on the rate with which binding occurs, while k_b depends primarily on the equilibrium value of p_{occ} and is indicative of the strength of the binding.

The forward and backward rate constants for streptavidin binding to 1B-DNA origami templates of Design I were calculated using yield data collected for a sequence of different incubation times (**Figure 6**). Equilibrium was reached in 3 h with only ≈60% of DNA origami containing four bound streptavidins, with a value of p_{occ} of 89.7% ± 3.7%. The forward and backward rate constants calculated from these data are (4.1 ± 0.3) × 10^3 L mol^{-1} s^{-1} and (5.0 ± 0.4) × 10^{-5} s^{-1} respectively, compared to 7 × 10^7 L mol^{-1} s^{-1} and 10^{-7} s^{-1} for free streptavidin/biotin.[26] k_f and k_b differ by factors of ≈10^{-4} and ≈10^2 respectively. These results from our detailed measurements are consistent with those obtained previously using ensemble techniques.[24–30] k_b is typically reduced significantly when one of the functional groups on biotin is used to attach the linker, as this reduces its ability to hydrogen bond inside the streptavidin binding pocket.[28,37]

The discrepancy in the forward reaction rates can be explained by considering the effect the translational and rotational diffusion coefficients have on reaction rate. The translational diffusion coefficient is inversely proportional to the hydrodynamic radius, R_H, of the object, and the rotational diffusion coefficient is inversely proportional to R_H^3 according to the Stokes–Einstein and Stokes–Einstein–Debye equations, respectively. The overall dependence of the forward reaction rate on size, which reflects the time needed for collisions to occur and for the correct orientation for binding to be achieved, can therefore be estimated to vary roughly as R_H^{-4}. If we assume that the reaction rate is dominated by the species that diffuses fastest, then we should expect the forward reaction rate for streptavidin–biotin in solution versus streptavidin-origami to scale as $[(R_H \text{ streptavidin})/(R_H \text{ biotin})]^{-4}$. Biotin has a radius of 0.3 nm and the radius of streptavidin is 3 nm,[17] so we would expect the reaction rate to be reduced by ≈10^{-4} for streptavidin binding to biotinylated origami. Similarly, the binding reaction between Qdots and origami must also be considered as one between objects much larger than the functional groups.[38] In this case, k_f is limited by the kinetics of translational and rotational diffusion of the Qdots and DNA origami: the radius of streptavidin coated-Qdots is ≈10 nm[23] whereas the DNA origami has dimensions of 70 nm × 100 nm × 2 nm. We therefore expect that the forward reaction rate for streptavidin-origami versus Qdot-origami to scale as $[(R_{H\ Qdot})/(R_{H\ streptavidin})]^{-4} \approx 10^{-2}$. Our simple estimate agrees well with the values observed for the streptavidin-origami case, but the observed forward rate coefficient for the Qdot-origami case is (2.7 ± 0.4) × 10^3 L mol^{-1} s^{-1}, only a factor of two smaller than the streptavidin case. However, we have not taken into account factors such as the presence of multiple streptavidins on each Qdot or the fact that the tethered biotins can explore interaction space more quickly than the origami as a whole. We note that our measured values are consistent with other observations of binding interactions between streptavidin and biotin-functionalized Qdots.[37]

The observed forward binding rate constant of Qdot-bound streptavidin and 3B-DNA origami- conjugated biotin is (2.0 ± 0.1) × 10^3 L mol^{-1} s^{-1}, similar to the 1B case, indicating that the addition of extra binding sites does very little to change the forward reaction rate. However, the backward reaction rate constants are (1.1 ± 0.2) × 10^{-4} s^{-1} and (6.0 ± 0.3) × 10^{-6} s^{-1} for the Qdot/1B and Qdot/3B cases respectively. These rates

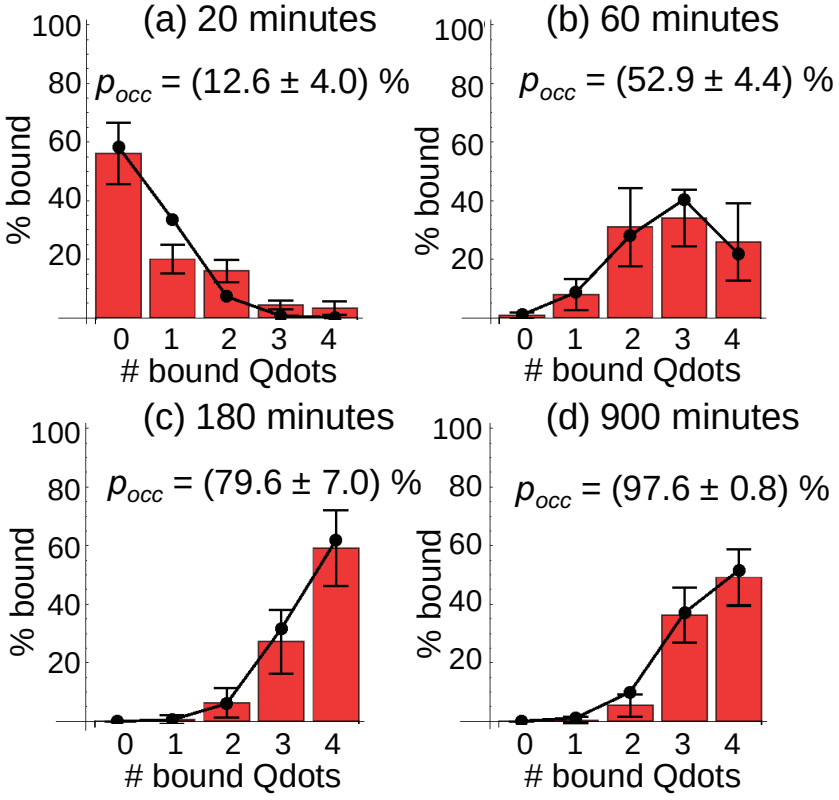

Figure 5. Histogram (bars) for the yield of Qdot patterns generated on 3B-DNA origami of Design I for different incubation times. a) 20 min, b) 60 min, c) 180 min, and d) 900 min. The mean values of p_{occ} were calculated using a least squares fit of the averaged data to a binomial distribution. The error bars are the 1 σ variation in the results from the separate AFM images for each time. The binomial distributions with these values, p_{occ} (quoted as mean ± 1 σ) are shown, as a guide to the eye, as solid lines.

differ by a factor of $\approx 5 \times 10^{-2}$. This difference is matched by the increase in p_{occ} from 70% to 97%.

The ratio of the forward and backward rate constants for Designs II and III can be determined from the equilibrium values of p_{occ} and the initial concentration of the DNA, $[DNA]_{init}$. For the process shown in Equation (1) we have at equilibrium

$$\frac{k_b}{k_f} = \frac{(15 - p_{occ})(1 - p_{occ})[DNA]_{init}}{p_{occ}} \quad (3)$$

The initial DNA concentration was the same in all cases and since p_{occ} is restricted to lie between 0 and 1 the factor $(15 - p_{occ})$ cannot vary significantly and so the ratio $k_b k_f^{-1}$ (i.e., K_d) scales predominantly as $(1 - p_{occ})p_{occ}^{-1}$. We therefore use the value of $(1 - p_{occ})p_{occ}^{-1}$ as a scaling factor to compare the effect of the different designs on Qdot binding. The results of this analysis are shown in **Table 1**.

The value of $(1 - p_{occ})p_{occ}^{-1}$ for the monovalent case varies by a small amount for the different designs, changing by a factor of ≈2 from Design I to Design II and by a factor of ≈4 from Design I to Design III. For the trivalent case, however, $(1 - p_{occ})p_{occ}^{-1}$ increases by 10 in going from Design I to Design II and by 20 in going from Design I to Design III. Since we can calculate only how the ratio $k_b k_f^{-1}$ scales for Designs II and III we obviously cannot determine separately how k_b and k_f change relative to Design I. However, for Design II the fact that the binomial fit to the data is within the error bars implies that a single value of p_{occ} and hence single values of k_b and k_f apply in that case. By comparison, we speculate that for Design III a single value of k_f cannot be used because of the strong steric hindrance and/or electrostatic effects discussed above.

2.5. More Flexible Linkages

As discussed above, the rate of Qdot–origami binding is relatively slow and is, at least in part, controlled by the time it takes for the biotin fixed on the origami and the streptavidin bound to the surface of Qdot to find the correct orientation for interaction.[17,28] In order to explore this in more detail, we systematically increased the length of the biotin-origami linker from 4 thymines (4T), to 6 thymines (6T), 8 thymines (8T), and 10 thymines (10T) for both the 1B and 3B cases to enable the biotin access to a progressively larger configuration space essentially independently of the motion of the origami to which it is attached. **Figure 7**b shows the results for the 3B case: the binding equilibrium is reached more rapidly as the linker length is increased, by a factor of ≈3.5 and ≈7 for the 6T and 8T cases, respectively. The same overall trend is observed for the 1B case. While values for k_b vary substantially, the values for K_d are all within a factor of ≈ 2 to 3, suggesting that the primary effect of the longer linker is to increase k_f, with minimal effect on affinity. As the linker length is increased, however, instances of unwanted binding events, including interactions of multiple origami with single Qdots for the singly-biotinylated designs and multiple Qdots binding to a single binding location in the triply-biotinylated origami appear also to increase (**Figure 8**). As a result, quantitative analysis of the 10T linker case was not possible. The creation of unwanted side products indicates that increased linker length as a strategy for increasing the reaction rate has limited utility. It may be possible to mitigate this effect by moving the Qdot binding locations away from the corners of the origami, thereby making them less accessible to the linkers on adjacent origami.

Table 1. Mean occupation probabilities, p_{occ}, and values of $(1 - p_{occ})$ p_{occ}^{-1} for the monovalent and trivalent versions of Designs I, II, and III.

	Monovalent p_{occ} [%]	Monovalent $(1 - p_{occ})$ p_{occ}^{-1}	Trivalent p_{occ} [%]	Trivalent $(1 - p_{occ})$ p_{occ}^{-1}
Design I	70.0	0.4	97.6	0.02
Design II	58.2	0.7	81.8	0.2
Design III	40.0	1.5	71.5	0.4

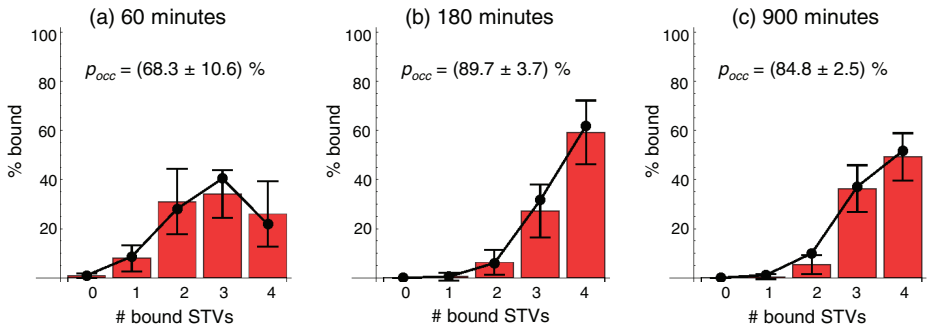

Figure 6. Histogram (bars) for the yield of streptavidin patterns generated on 1B-DNA origami of Design I for different incubation times. a) 60 min, b) 180 min, and c) 900 min. The values of p_{occ} were calculated using a least squares fit of the data to a binomial distribution. The error bars are the 1 σ variation in the results from the separate AFM images for each time, computed using a least squares fit of the data to a binomial distribution. The binomial distributions with these values, p_{occ} (quoted as mean ± 1 σ) are shown, as a guide to the eye, as solid lines. Equilibrium was reached in 3 h, the difference between (b) and (c) being within the error bars.

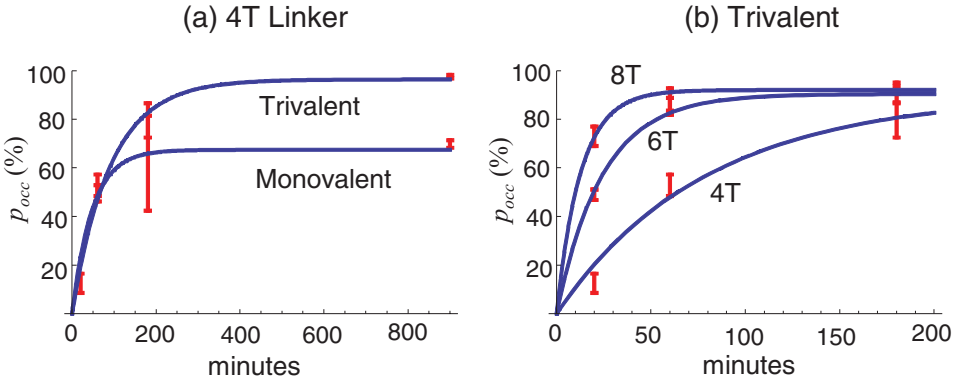

Figure 7. Graphs of p_{occ} as a function of incubation time. a) The graph shows the 4 thymine (4T) linker case, comparing singly biotinylated binding locations (monovalent) to triply biotinylated binding locations (trivalent). In this case the values of k_f stay the same but the equilibrium value of p_{occ} is significantly smaller for the single biotin case. b) The graph shows the trivalent binding location case for three linker lengths, 4 thymine (4T), 6 thymine (6T), and 8 thymine (8T). Increasing the linker length increases k_f without significantly changing the equilibrium value of p_{occ}, which is close to 100% in all cases. The values of k_f and k_b were determined using a least squares fit. This minimizes $\sum(p_{occ,i} - p_{occ}(t_i))^2$ with respect to k_f and k_b where $p_{occ,i}$ are the measured values of the binding efficiency (red dots) at times t_i and the blue curves are the plots of the function $p_{occ}(t)$ using the fitted values of k_f and k_b. The errors or uncertainties in the values of k_f and k_b were determined by using the least squares equations themselves to determine the sensitivity of k_f and k_b to variations in the measured values of $p_{occ,i}$.

3. Conclusions

We have performed a quantitative exploration of the parameters that affect the kinetics and yield of streptavidin-biotin mediated Qdot binding to DNA origami, and have found the following results. First, multivalent binding locations provide a dramatic improvement, increasing the yield from 22.1% ± 6.5% to 90.2% ± 3.3% as the valency goes from one biotin per binding location to three biotins per binding location. Second, longer linkers increase the reaction rate, but can lead to poorer quality structures and undesirable side products. Third, steric hindrance effects that lead to poor placement precision extend to approximately twice the hydrodynamic radius of the Qdots, significantly limiting the minimum spacing that can be achieved. Although these findings are for a specific system, they likely apply more broadly to self-assembly processes using DNA as a templating structure.

We have demonstrated a quantitative methodology for the analysis of time course data to extract forward and backward reaction rate coefficients. This provides considerable physical insight into the kinetics of these types of self-assembly processes. The K_d of the DNA-nanoparticle complex is up to seven orders of magnitude larger than that of the native biotin–streptavidin complex. This disparity arises from the fact that the combined dependence of the translational and rotational diffusion constants on object radius varies as the inverse fourth power. Thus, a small change in the size of the objects being assembled has a dramatic impact on the forward reaction rates, reflected by the rate with which a given assembly process reaches completion.

Our data therefore suggest that purely diffusion-driven self-assembly methods are likely to be limited in terms of rate and yield as the sizes of the components being assembled increases.

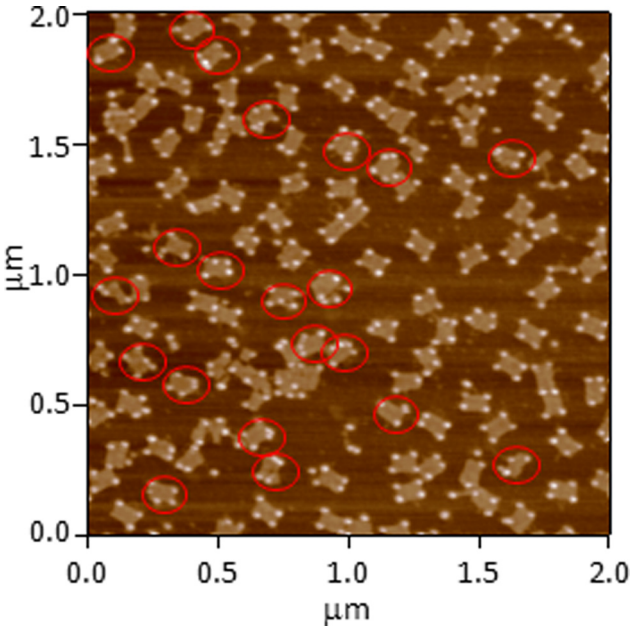

Figure 8. AFM image of quantum dot nanopattern assembled on DNA origami templates with longer linkers after 20 min incubation with 3B-origami of 10T linkers. DNA origami displaying multiple quantum dots at one binding location are highlighted in red.

4. Experimental Section

Materials: A single strand M13mp18 (catalog number: N4040S) was purchased from New England Biolab.[22] All unmodified and biotin labeled staple strands were purchased commercially[22] and used without further purification. The streptavidin modified Qdot solution and all other chemicals were purchased commercially.[22]

Self-Assembly of DNA Origami: Rectangular DNA origami was assembled according to the original design by Rothemund.[4] A long single strand of M13mp18 and stapler strands were mixed at molar ratio of 1:5 in 1× TAE/Mg^{2+} buffer (40 mmol L^{-1} (mM) tris(hydroxymethyl) aminomethane (tris), 20 mmol L^{-1} (mM) acetic acid, 2 mmol L^{-1} (mM) ethylenediaminetetraaceticacid (EDTA), and 12.5 mmol L^{-1} (mM) magnesium acetate, pH 8.0) and slowly annealed at 1°C min^{-1} from 95 °C to room temperature using a DNA thermal cycler. Excess staple strands were removed by washing four to five times with 1× TAE/Mg^{2+} buffer (400 μL) in a 100 000 molecular weight cutoff filter (100 kDa MWCO) centrifuge filter at 3500 × g for 2 min in a microcentrifuge. To avoid stacking of origami along vertical edges, staple strands on vertical edges have been omitted.

Preparation and AFM Imaging of Qdot-DNA Origami Conjugates: DNA origami solution (1.5 nmol L^{-1}, 3 μL) was loaded on freshly cleaved mica surface and left to adsorb on the surface for ≈1 min and dried by gentle blowing with compressed air. The Qdot solution was added on the origami sample at 15× molar ratio to the binding locations on an origami and incubated for 15 h, unless otherwise stated, in a Petri dish with moist wipes at room temperature. After incubation, unbound Qdots were washed away with deionized water and the sample was dried again.

To verify that the procedures to create the conjugates leave a significant fraction of the DNA origami on the mica surface, we calculated the expected number of origami per surface area on the basis of the origami concentration in the applied solution and compared that to our experimental results. A drop of DNA origami solution (3 μL) contains roughly 3×10^9 origami. When deposited on mica, this volume makes a spot with a diameter of 0.8 cm to 1 cm. If all of the origami in the drop settle on the mica surface and remain adsorbed after drying, the density of origami should be about 20 μm^{-2} to 30 μm^{-2}. The AFM images usually cover a 9 μm^{-2} area, which means that each image should contain about 200 origami. The number of discrete origami detected in each image ranged from 30 to 140, showing that about 10% to 80% of the origami remains on the mica surface.

AFM imaging was performed under dry conditions in tapping mode with standard silicon cantilevers (PPP-NCH) with a nominal spring constant of 42 N m^{-1} (range of 10 N m^{-1} to130 N m^{-1}) and resonance frequency between 204 kHz and 497 kHz.[22,39] The tip–surface interaction was minimized by optimizing the scan set point. It was verified that the AFM imaging process did not perturb the dot-origami complexes by performing repeated scans of the same area and confirming that the first and last images were effectively identical. To ensure adequate statistics, more than 240 origami were counted in multiple (between 4 and 8) AFM images.

Supporting Information

Supporting Information is available from the Wiley Online Library or from the author.

Acknowledgements

The authors thank Veronika Szalai and Paul W. K. Rothemund for discussions and theoretical insights. The authors also thank Rachel Cannara and Zhao Deng for allowing us to use the AFM.

Received: September 3, 2011
Revised: November 18, 2011
Published online: January 17, 2012

[1] N. C. Seeman, *Mol. Biotechnol.* **2007**, *37*, 246.
[2] T. LaBean, H. Li, *Nano Today* **2007**, *2*, 26.
[3] C. M. Niemeyer, U. Simon, *Eur. J. Inorg. Chem.* **2005**, *2005*, 3641.
[4] P.W. K. Rothemund, *Nature* **2006**, *440*, 297.
[5] R. D. Barish, R. Schulman, P. W. K. Rothemund, E. Winfree, *Proc. Natl. Acad. Sci. USA* **2009**, *106*, 6054.
[6] W. Liu, H. Zhong, R. Wang, N. Seeman, *Angew. Chem. Int. Ed.* **2011**, *50*, 264.
[7] M. Endo, T. Sugita, Y. Katsuda, K. Hidaka, H. Sugiyama, *Chem. Eur. J.* **2010**, *16*, 5362.
[8] R. J. Kershner, L. D. Bozano, C. M. Micheel, A. M. Hung, A. R. Fornof, J. N. Cha, C. T. Rettner, M. Bersani, J. Frommer, P. W. K. Rothemund, G. M. Wallraff, *Nat. Nanotechnol.* **2009**, *4*, 557.
[9] J. Sharma, R. Chhabra, C. S. Andersen, K. V. Gothelf, H. Yan, Y. Liu, *J. Am. Chem. Soc.* **2008**, *130*, 7820.
[10] L. A. Stearns, R. Chhabra, J. Sharma, Y. Liu, W. T. Petuskey, H. Yan, J. C. Chaput, *Angew. Chem. Int. Ed.* **2009**, *48*, 8494.
[11] A. M. Hung, C. M. Micheel, L. D. Bozano, L. W. Osterbur, G. M. Wallraff, J. N. Cha, *Nat. Nanotechnol.* **2010**, *5*, 121.
[12] S. Pal, Z. Deng, B. Ding, H. Yan, Y. Liu, *Angew. Chem. Int. Ed.* **2010**, *49*, 2700.
[13] B. Ding, Z. Deng, H. Yan, S. Cabrini, R. N. Zuckermann, J. Bokor, *J. Am. Chem. Soc.* **2010**, *132*, 3248.
[14] H. Bui, C. Onodera, C. Kidwell, Y. Tan, E. Graugnard, W. Kuang, J. Lee, W. B. Knowlton, B. Yurke, W. L. Hughes, *Nano Lett.* **2010**, *10*, 3367.
[15] S. Rinker, Y. Ke, Y. Liu, R. Chhabra, H. Yan, *Nat. Nanotechnol.* **2008**, *3*, 418.
[16] B. Ding, H. Wu, W. Xu, Z. Zhao, Y. Liu, H. Yu, H. Yan, *Nano Lett.* **2010**, *10*, 5065.

[17] P. C. Weber, D. H. Ohlendorf, J. J. Wendoloski, F. R. Salemme, *Science* **1989**, *243*, 85.
[18] A. Chilkoti, P. S. Stayton, *J. Am. Chem. Soc.* **1995**, *117*, 10622.
[19] M. L. Jones, G. P. Kurzban, *Biochemistry* **1995**, *34*, 11750.
[20] T. Sano, C. R. Cantor, *J. Biol. Chem.* **1990**, *265*, 3369.
[21] L. E. Morrison, L. M. Stols, *Biochemistry* **1993**, *32*, 3095.
[22] The full description of the procedures used in this paper requires the identification of certain commercial products and their suppliers. The inclusion of such information should in no way be construed as indicating that such products or suppliers are endorsed by NIST or are recommended by NIST or that they are necessarily the best materials, instruments, or suppliers for the purposes described.
[23] Qdot Streptavidin Conjugates, Molecular Probes, Inc. **2007**, 1.
[24] T. Buranda, G. P. Lopez, J. Keij, R. Harris, L. A. Sklar, *Cytometry* **1999**, *37*, 21.
[25] J. A. Thompson, H. H. Bau, *J. Chromatogr. B* **2010**, *878*, 228.
[26] C. Ku, B. B. Lentrichia, *J. Colloid Int. Sci.* **1989**, *132*, 578.
[27] D. Eberbeck, C. Bergemann, F. Wiekhorst, U. Steinhoff, L. Trahms, *J. Nanobiotechnol.* **2008**, *6*, 1.
[28] T. Buranda, G. M. Jones, J. P. Nolan, J. Keij, G. P. Lopez, L. A. Sklar, *J. Phys. Chem. B* **1999**, *103*, 3399.
[29] S. Huang, M. D. Stump, R. Weiss, K. D. Caldwell, *Anal. Biochem.* **1996**, *237*, 115.
[30] S. Zhao, W. M. Reichert, *Langmuir* **1992**, *8*, 2785.
[31] N. V. Voigt, T. Tørring, A. Rotaru, M. F. Jacobsen, J. B. Ravnsbék, R. Subramani, W. Mamdouh, J. Kjems, A. Mokhir, F. Besenbacher, K. V. Gothelf, *Nat. Nanotechnol.* **2010**, *5*, 200.
[32] W. Shen, H. Zhong, D. Neff, M. L. Norton, *J. Am. Chem. Soc.* **2009**, *131*, 6660.
[33] M. Pilo-Pais, S. Goldberg, E. Samano, T. H. LaBean, G. Finkelstein, *Nano Lett.* **2011**, *11*, 3489.
[34] Purchased from Invitrogen (Qdot 605 Streptavidin conjugate).
[35] N. Wu, X. Zhou, D. M. Czajkowsky, M. Ye, D. Zeng, Y. Fu, C. Fan, J. Hu, B. Li, *Nanoscale* **2011**, *3*, 2481.
[36] J. N. Israelachvili, *Intermolecular & Surface Forces*, 2nd ed. Academic Press, London **1991**, Ch.13.
[37] C. K. Chignell, D. K. Starkweather, B. K. Sinha, *J. Biol. Chem.* **1975**, *250*, 5622.
[38] J. L. Swift, R. Heuff, D. T. Cramb, *Biophys. J.* **2006**, *90*, 1396.
[39] Purchased from Nanosensors.